AD-A064 548 BATTELLE COLUMBUS LABS OHIO F/G 17/4
ANALYSIS OF A MODEL FOR IR SUPPRESSION.(U)
SEP 78 R P KENAN, G WOLKEN, J MCCREERY F49620-77-C-0056
UNCLASSIFIED AFOSR-TR-79-0009 NL

| OF |
AD A064548

END
DATE FILMED
4-79
DDC

Battelle
Columbus Laboratories

LEVEL II

Report

AIR FORCE OFFICE OF SCIENTIFIC RESEARCH (AFSC)
NOTICE OF TRANSMITTAL TO DDC
This technical report has been reviewed and is approved for public release IAW AFR 190-12 (7b).
Distribution is unlimited.
A. D. BLOSE
Technical Information Officer

ANALYSIS OF A MODEL FOR IR SUPPRESSION

to

AIR FORCE OFFICE OF SCIENTIFIC RESEARCH
BOLLING AFB, WASHINGTON, D.C.

September 29, 1978

by

R. P. Kenan, G. Wolken, J. McCreery,
R. Barnes, D. Applebaum and G. Whitacre

See 1473

F49620-77-C-0056

TABLE OF CONTENTS

LIST OF TABLES

LIST OF FIGURES

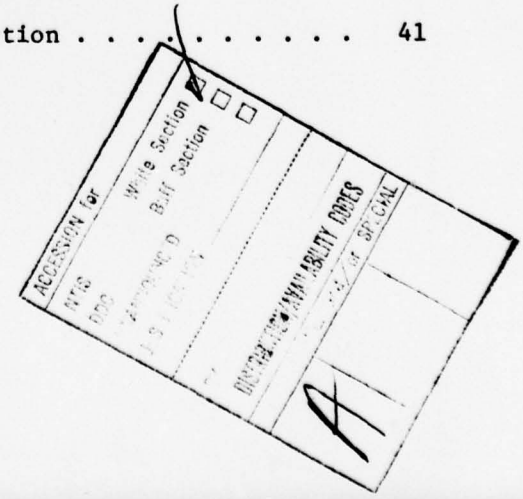

FINAL REPORT

on

ANALYSIS OF A MODEL FOR IR SUPPRESSION

to

AIR FORCE OFFICE OF SCIENTIFIC RESEARCH
BOLLING AFB, WASHINGTON, D.C.

from

BATTELLE COLUMBUS LABORATORIES
COLUMBUS, OHIO

September 29, 1978

INTRODUCTION

This project originated in a search to find mechanisms to explain the data obtained at AFCRL[1] on the efficacy of lampblack in reducing the infrared (2-5 μm) signature of aircraft jet engines. These data were taken primarily on stationary aircraft with a variety of lampblack injection rates. While the tail-on results were readily explained as due to simple absorption by the lampblack, the range of injection rates and aspect angles considered appeared to require unusually high absorption coefficients for carbon. Because the cloaking effect was effective at all angles, it did not seem likely that the effect was due to scatter, since radiation scattered from one direction would then appear at other directions, so there would be "hot" regions. Cooling because of the sheer mass of carbon was not a sensible solution because of the variety of mass injection rates over which the effect operated and because of the disparity in the carbon-to-fuel mass injection ratios encountered in military aircraft.

One promising candidate was a radiationless de-excitation (quenching) of CO_2 (and also H_2O) molecules on the surface of the carbon particles. It was assumed that the lampblack mixed with the hot outer gases of the exhaust plume in a thin shrouding layer surrounding the hottest portion of the exhaust. In this region, the CO_2 molecules would interact by collision with the surface of the carbon particles, losing their excitation energy to internal and motional degrees of freedom of the particles. If this de-excitation took place rapidly,

many CO_2 molecules would be de-excited on each particle. The particle flow would carry the energy away rapidly to be dissipated in the atmosphere. At the same time, the de-excited CO_2 molecules would behave like a resonant absorber, removing radiative energy and delivering it to the carbon. The net effect of this cyclic process would presumably be an apparently enhanced absorption coefficient for the carbon particles.

The objects of the project are

- to examine the quenching process from a theoretical viewpoint to obtain estimates of de-excitation rates to be expected.
- to conduct a simple experiment to measure the extinction coefficient of lampblacks in a static matrix.
- to calculate the expected signature of a real jet aircraft, in flight, with and without the quenching mechanism activated.

From the results of these three tasks a conclusion is to be reached on the significance of the mechanism to infrared signature suppression.

In the following section of the report, the theoretical analysis of the quenching of CO_2 and H_2O molecules on carbon surfaces is presented. Next the experimental characterization of several typical lampblacks is described. Then the signature calculations and an analytical model are presented. Concluding comments on the mechanism and its significance are given in the final section.

QUENCHING OF INFRA-REF EMISSIONS OF CO_2, H_2O BY COLLISIONS WITH GRAPHITE

Summary

We have performed computer simulations for the collisions of vibrationally excited CO_2 and H_2O with a graphite surface. A model potential was developed to describe the interaction between CO_2, H_2O and the basal plane of graphite. This potential was calibrated against known bond strengths and other properties for the isolated molecules (CO_2, H_2O) and fragements (CO, O_2, H_2, OH). Data for the interaction of the molecules, fragments, and individual atoms (C, H, O) interacting with the basal plane of graphite were also utilized. In so far as these bonding properties are accurately known, our model potential reproduces them.

Using this model potential, classical trajectories were calculated to simulate collisions of vibrationally excited CO_2 and H_2O with the basal plane of graphite. The basal plane is not usually the most reactive chemical site on a graphite particle, but, statistically, is usually the most abundantly exposed plane and, hence, will collide most frequently with gas molecules. However, the edge planes seem to bind adsorbed particles more tightly than the basal plane. Restricting attention to the basal plane would tend to underestimate quenching.

Since the interaction potential is quite realistic, the trajectories are rather long to compute. As a result, only a handful could be studied for the various gas conditions, surface temperature, and other collision parameters. However, the results uniformly predict that when a vibrationally excited CO_2 or H_2O (i.e., a potential IR emitter) collides with a graphite surface, it will be destroyed as an emitter. While there is some variation in the actual outcome of the collisions, the one result not observed for any of the cases studied is elastic rebound (with the possibility of subsequent IR emission). Given the uncertainties in sample size our best estimates for collisional quenching probability is 0.8-1.0 independent of gas or surface temperatures.

In a realistic case, the graphite surface will be covered to an unknown extent with adsorbed contaminants. Other work in gas solid energy

transfer has shown that adsorbed species with vibrational characteristics similar to the gas molecules (i.e., a near-resonant energy transfer process) will lead to enhanced quenching. Thus, we believe that the simplifications in our model will tend to underestimate quenching, lending further credibility to our conclusions.

Potential: General Discussion

The details of this model potential for the interaction of triatomic molecules with a solid surface are given in our previous work.[2] We briefly review the appropriate formulas here. We are interested in the interaction of H_2O of CO_2 with the basal plane of graphite. While probably not the most reactive face of graphite, it is usually exposed to a greater extant than any other. Hence, it is most likely to undergo collisions with gas molecules. As indicated below, our results indicate that the basal plane is a very efficient quencher. One would expect that more reactive sites (e.g. edge planes) would be certainly no less efficient and probably more efficient due to the larger bond strengths. Following our previous work, we use a London-Eyring-Polanyi-Sato type potential function for the gas-solid interaction. This potential function, for three atoms interacting with a solid surface, is given by the five linear independent valence bond structures that correspond to maximum bonding in the ground state of a six-electron system (see Figure 1a). The energy of the system is given by the generalized eigenvalue equation

$$\underset{\sim}{HC} = \underset{\sim}{SCE} \tag{1}$$

where the matrix elements H_{ij}, S_{ij} are between the bond eigenfunctions $\underset{\sim}{I}_1,\ldots,\underset{\sim}{I}_5$ shown in Figure 1a. There are just six two-body interactions that are relevant to the triatom-solid surface problem: three atom-atom interations and three atom-surface interations. These are shown in Figure 1b. All other interactions that occur in the six-electron problem are set to zero here. This implies a model of the solid in which, as an extended source of the electrons required for bonding, it can provide the necessary electrons at any point or points on the surface. Assuming that the one-electron orbitals of the system are mutually orthogonal, we obtain the matrix elements

$$H_{11} = 8Q + 8[(ab) + (cd)] - 4[(bc) + (ac) + (af) + (be)]$$

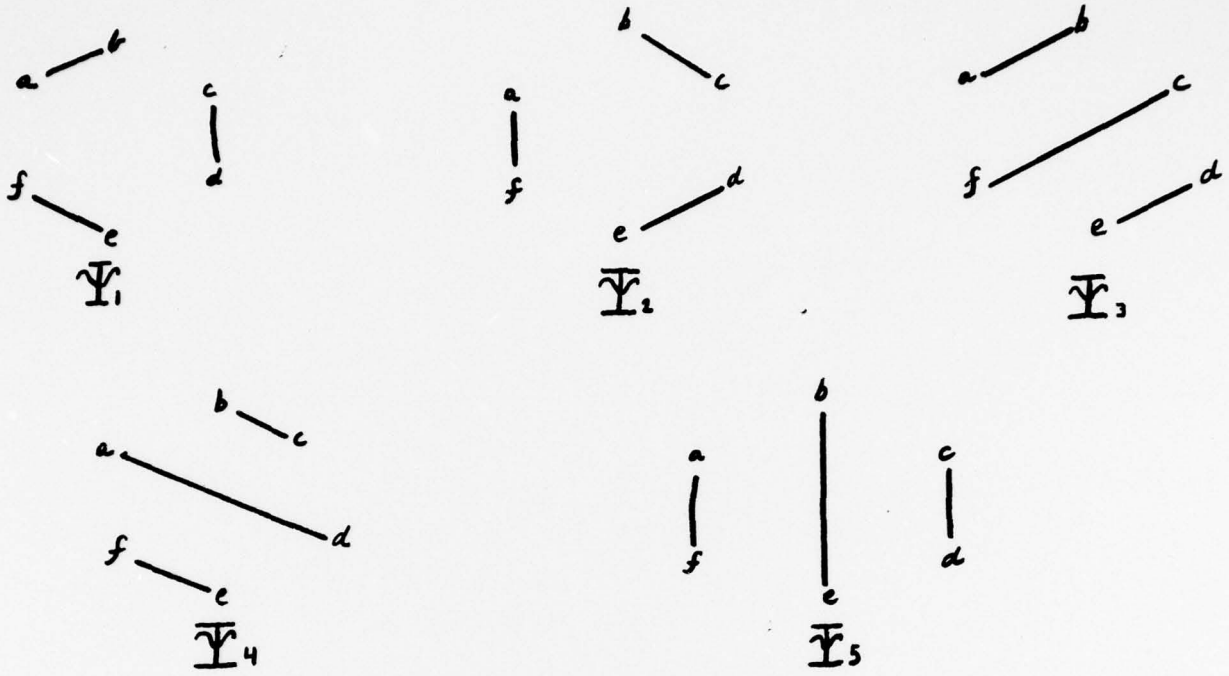

Figure 1a: Valence bond structures for a six-electron system.

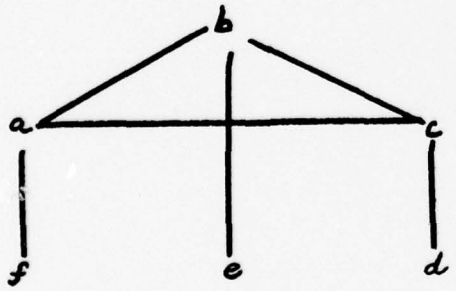

Figure 1b: Two-body interactions for a triatom-solid surface system: a, b, c represent gas-phase atoms; d, e, f represent electrons of the solid surface.

$$H_{22} = 8Q + 8[(bc) + (af)] - 4[(ab) + (ac) + (be) + (cd)]$$

$$H_{33} = 8Q + 8(ab) - 4[(bc) + (ac) + (af) + (be) + (cd)] \qquad (2)$$

$$H_{44} = 8Q + 8(bc) - 4[(ab) + (ac) + (af) + (be) + (cd)]$$

$$H_{55} = 8Q + 8[(af) + (be) + (cd)] - 4[(ab) + (bc) + (ac)]$$

$$H_{12} = H_{34} = H_{35} = H_{45} = 2Q + 2[(ab) + (bc) + (af) + (be) + (cd)] - 4(ac)$$

$$H_{13} = -4Q - 4[(ab) + (cd)] + 2[(bc) + (ac) + (af) + (be)]$$

$$H_{14} = -4Q - 4[(ab) + (bc) - 2(ac) + (cd)] + 2[(af) + (be)]$$

$$H_{15} = -4Q - 4[(ab) + (af) + (be) + (cd)] + 2[(bc) + (ac)]$$

$$H_{23} = -4Q - 4[(ab) + (bc) - 2(ac) + (af)] + 2[(be) + (cd)]$$

$$H_{24} = -4Q - 4[(bc) + (af)] + 2[(be) + (cd) + (ab) + (ac)]$$

$$H_{25} = -4Q - 4[(bc) + (af) + (be) + (cd)] + 2[(ab) + (ac)]$$

where Q is the Coulomb integral

$$Q = (abcdef|H|abcdef) \qquad (3)$$

and (ab) etc. are the exchange integrals. The overlap matrix elements are given by

$$S_{11} = S_{22} = S_{33} = S_{44} = S_{55} = 8$$

$$S_{12} = S_{34} = S_{35} = S_{45} = 2 \qquad (4)$$

$$S_{13} = S_{14} = S_{15} = S_{23} = S_{24} = S_{25} = -4$$

It is supposed that the Coulomb integral Q can be adequately represented as a sum of two-body Coulomb integrals $Q = \sum_{ij} Q_{ij}$, and that the exchange integrals may be written as two-body exchange integrals. As in the usual LEPS treatment we assume that atom-atom and atom-surface interactions can be described by Morse potentials. We obtain

$$Q_{ij} = \frac{1}{4(1+\Delta_{ij})} \{(3+\Delta_{ij}) \exp(-2\alpha_{ij}(r_{ij} - r_{ij}^{o})) -$$

$$(2+6\Delta_{ij}) \exp(-\alpha_{ij}(r_{ij} - r_{ij}^{o}))\}$$

(5)

$$(ij) = \frac{1}{4(1+\Delta_{ij})} D_{ij} \{(1+3\Delta_{ij}) \exp(-2\alpha_{ij}(r_{ij} - r_{ij}^{o})) -$$

$$(6+2\Delta_{ij}) \exp(-\alpha_{ij}(r_{ij} - r_{ij}^{o}))\}$$

where D_{ij}, α_{ij}, r_{ij}^{o}, and Δ_{ij} are the dissociation energy, Morse parameter, equilibrium distance, and Sato parameter for the i-j interaction, and r_{ij} is the i-j distance. Thus, the matrix elements in equation (1) are determined and hence the energy E. The ground-state energy is the lowest eigenvalue of equation (1).

To study the dynamics of gas-solid interactions, we use the classical trajectory method of stepwise integration of the classical equations of motion. For this, we require the derivatives of the energy with respect to the three coordinates of each atom. These derivatives are obtained from equation (1) by the matrix Hellmann-Feynman theorem:

$$\frac{\partial \underset{\sim}{E}}{\partial R} = (\underset{\sim}{C}^{+} \underset{\sim}{S} \underset{\sim}{C})^{-1} \underset{\sim}{C}^{+} \frac{\partial \underset{\sim}{H}}{\partial \underset{\sim}{R}} \underset{\sim}{C} \qquad (6)$$

$\frac{\partial \underset{\sim}{H}}{\partial R}$ is obtained by differentiating each of the matrix elements of $\underset{\sim}{H}$. The eigenvectors $\underset{\sim}{C}$ are obtained in the solution of the generalized eigenvalue equation (1) and so the derivatives $\frac{\partial E}{\partial R}$ and hence the forces on each atom are easily evaluated at each step in the trajectory.

This potential assumes a model of the surface in which the atoms of the solid are fixed at their equilibrium positions and are not allowed to move. No energy transfer between the gas atoms and the solid surface

is permitted and energy terms associated with geometry changes in the substrate atoms are neglected. For the interaction of H_2O and CO_2 with graphite, we are interested in possible energy transfer to the solid and so we must relax this rigid surface restrictions. The detailed generalization of this model to include gas-solid energy transfer was effected under a separate AFOSR contract (F49620-77-C-0004). The results have been reported elsewhere[3] and will be briefly summarized here. Using the same basic potential, V_{LEPS}, as described above, we include additional terms to account for the motion of the solid atoms. These correction terms are:

(1) V_r, the restoring force on each atom of the solid, tending to return it to its lattice site.

(2) V_{corr}, to account for the change in the gas-surface interaction when the solid atom is displaced from its lattice site.

We have

$$V_{total} = V_{LEPS} + V_r + V_{corr} \tag{7}$$

V_r and V_{corr} must vanish when all the solid atoms occupy their lattice positions. We have used pair-potentials for V_r and V_{corr} to correct V_{LEPS} approximately to allow for the motion of the solid atoms. Assuming that V_r binds the solid atom to its lattice site via a harmonic potential constitutes an Einstein model of the solid. This was used in the present work.

This model does not include the non-additive corrections for the solid-solid interactions, nor does it include the non-additive corrections to V_{corr}. For the restoring force V_r we have used a harmonic potential binding an atom of the solid to its fixed lattice site. To account for the change in the gas-solid potential due to displacement of the surface atom from its lattice site, we have used a pair-potential for V_{corr} connecting each gas atom with each of the surface atoms that are allowed to move. V_{LEPS} already contains the interaction of each gas atom with each lattice site, so to avoid including it twice, this lattice site interaction must be subtracted from V_{corr}. We take

$$V_{corr} = \sum_{g}^{Ng} \sum_{s}^{Ns} [W(R_{g-s}) - W(R_{g-\ell})] \qquad (8)$$

where N_g is the number of gas atoms, N_s is the number of solid atoms that are free to move, R_{g-s} is the distance between the gas atom and the solid atom, and $R_{g-\ell}$ is the distance between the gas atom and the lattice site of the solid atom. As required, if the surface atom occupies its lattice site

$$R_{g-s} = R_{g-\ell} \quad \text{and} \quad V_{corr} = 0 \quad .$$

The total gas-solid potential for the moving surface case is

$$V_{total} = V_{LEPS} + \sum_{s}^{Ns} V_R^s + \sum_{\theta}^{Ng} \sum_{s}^{Ns} [W(R_{g-s}) - W(R_{g-\ell})] \qquad (9)$$

where V_R^s is the harmonic restoring force for solid atoms s.

In summary, the triatom-solid surface potential that we have used for the study of CO_2-graphite and H_2O-graphite interactions includes

(1) all forces, pairwise and non-pairwise, to describe the interaction of a gas molecule with a surface when the surface atoms are fixed at their lattice sites.

(2) pairwise corrections for the motion of the solid atoms away from their lattice sites.

(3) pairwise corrections to account for the change in the gas-solid potential due to displacement of the surface atoms from their lattice sites.

Potential: CO_2 + Graphite, H_2O + Graphite

To use the potential described above for H_2O and CO_2 interacting with the basal plane of graphite, we require Morse and Sato parameters for each of the atom-atom and atom-solid interactions. The values of the Morse parameters used for the H-H, H-O, C-O, and O-O interactions are readily available from spectroscopic data and are given in Table I. The Sato parameters Δ for C-O and O-O in CO_2 were chosen to be 0.3 and 0.1 respectively.

TABLE I

Morse parameters (in atomic units) for diatomic interactions.

	O-H	H-H	C-O	O-O
D_o	0.1697	0.1744	0.4132	0.1903
α	1.2119	1.0277	1.2170	1.4100
r_o	1.8341	1.4016	2.1320	2.2820

For H_2O the three atom LEPS potential was that supplied by A. Gauss (U.B. Army Ballistic Research Laboratories) which the Sato parameters are equal and are given by

$$\Delta = 100\{\sin^6\left(\frac{6\theta}{7}\right) + \frac{3}{4}\sin^4\left(\frac{\theta}{2}\right)\}\sin^{16}(2\phi)(R_1R_2)^4 e^{-4R_1R_2} \qquad (10)$$

where R_1 and R_2 are the O-H distances (in a.u.), θ is the angle $H\hat{O}H$ and $\phi = \arctan(R_1/R_2)$. This Δ function gives rise to an H_2O LEPS potential in which the equilibrium geometry and binding energy are close to the experimental values.

For the atom-solid interactions, the Morse parameters are chosen to be functions of x and y, where the x-y plane is parallel to the plane of the graphite surface. To reflect the symmetry of the basal plane of graphite, we chose the Morse parameters at a point (x,y,z) to be

$$\begin{aligned} D_o = a + \frac{b}{3}\{&\cos(\beta R_{a1}) + \cos(\beta R_{a2}) + \cos(\beta R_{a3}) + \cos(\beta R_{b1}) + \\ &\cos(\beta R_{b2}) + \cos(\beta R_{b3}) + \cos(\beta R_{a1})\cos(\beta R_{b1}) + \\ &\cos(\beta R_{a2})\cos(\beta R_{b2}) + \cos(\beta R_{a3})\cos(\beta R_{b3})\} + \frac{c}{3}\{[\cos^2(\beta R_{a1})-1] \\ &[\cos^2(\beta R_{b1})-1] + [\cos^2(\beta R_{a2})-1][\cos^2(\beta R_{b2})-1] + [\cos^2(\beta R_{a3})-1] \\ &[\cos^2(\beta R_{b3})-1]\}, \end{aligned} \qquad (11)$$

and

$$\begin{aligned} r_o = d + \frac{e}{3}\{&\cos(\beta R_{a1}) + \cos(\beta R_{a2}) + \cos(\beta R_{a3}) + \cos(\beta R_{b1}) + \\ &\cos(\beta R_{b2}) + \cos(\beta R_{b3}) + \cos(\beta R_{a1})\cos(\beta R_{b1}) + \\ &\cos(\beta R_{a2})\cos(\beta R_{b2}) + \cos(\beta R_{a3})\cos(\beta R_{b3})\} + \frac{f}{3}\{[\cos^2(\beta Ra1)-1] \\ &[\cos^2(\beta R_{b1})-1] + [\cos^2(\beta R_{a2})-1][\cos^2(\beta R_{b2})-1] + [\cos^2(\beta R_{a3})-1] \\ &[\cos^2(\beta R_{b3})-1]\} \end{aligned} \qquad (12)$$

where

$$\begin{aligned} R_{a1} &= -y - \frac{x}{\sqrt{3}} & R_{a3} &= \frac{2x}{\sqrt{3}} & R_{b2} &= \frac{x}{\sqrt{3}} + y \\ R_{a2} &= \frac{x}{\sqrt{3}} - y & R_{b1} &= \frac{2x}{\sqrt{3}} & R_{b3} &= y - \frac{x}{\sqrt{3}} \end{aligned} \qquad (13)$$

and

$$\beta = \frac{2\pi}{s\sqrt{3}}$$

where s is the graphite nearest neighbor bond distance (= 2.68 a.u.). The parameters a, b, c, d, e, and f are chosen for each atom-graphite interaction by fitting the above functional forms to binding energies and equilibrium heights above the surface for each atom in bridge, on-top, and hole sites above the surface. The values used were taken from CNDO calculations of Messmer[4] and of Hayns[5] with the binding energies scaled to 0.2 of the calculated values as they suggest. Figure 2 shows the different sites of approach used; Table II gives the scaled values of Messmer and Haynes as used in these calculations. The resulting parameters are given in Table III. The Morse parameter α for the atom-graphite interactions is determined by fitting the potential energy curve at one of the binding sites to a parabola in the z direction; this gives

$$\alpha = \sqrt{\frac{\alpha_o}{D_o(\text{a.u.})}} \tag{14}$$

where α_o = 0.10585 for H, 0.12603 for O, and 0.1392 for C on graphite.

The Sato parameters for the atom-graphite interactions were chosen to be 0.0 for H and O in H_2O, -0.1 for O in CO_2, and -0.1 for C in CO_2 on graphite. Figures [3-5] are equipotential contour plots of CO_2 and H_2O approaching the graphite surface with the parameter values as given above and with the surface atoms in their equilibrium positions.

The restoring force for the solid atoms was chosen to be a harmonic oscillator with force constant determined by the temperature of the surface. The gas-solid atom and gas-lattice site potentials in the correction term V_{corr} were chosen as exponential repulsion terms

$$W = D\, e^{-\alpha(r-r_o)} \tag{15}$$

where D, α, and r_o were chosen to be the same as in the gas-solid Morse potential for the atom above an on-top site of the solid.

Classical Trajectories: Methods

With an approximate potential surface, we can now integrate classical equations of motion for the collision of the triatomic molecules

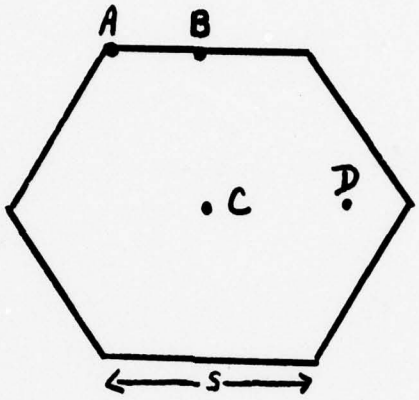

Figure 2. On-top (A), bridge (B) hole (C) and intermediate (D) sites for the approach of a gas-phase atom to the graphite surface. s is the nearest neighbor internuclear distance (= 2.68 a.u.).

TABLE II

Binding energies (in eV) and equilibrium heights above the surface (in Å) at different sites on the graphite surface.

	Bridge	On-Top	Hole
		H - Graphite	
Energy	0.85	0.82	0.11
Distance	1.0	1.2	0.5
		O - Graphite	
Energy	2.59	1.82	1.09
Distance	1.2	1.5	1.0
		C - Graphite	
Energy	4.08	4.52	6.53
Distance	1.2	1.3	0.6

TABLE III

Parameter values (in a.u.) for atom-graphite interactions.

	H - Graphite	O - Graphite	C - Graphite
a	0.0244	0.0814	0.1846
b	-0.0068	-0.0138	0.0185
c	0.0011	-0.0442	-0.0370
d	1.6535	2.2393	2.0790
e	-0.2362	-0.1228	-0.2830
f	0.7770	0.7937	0.4610

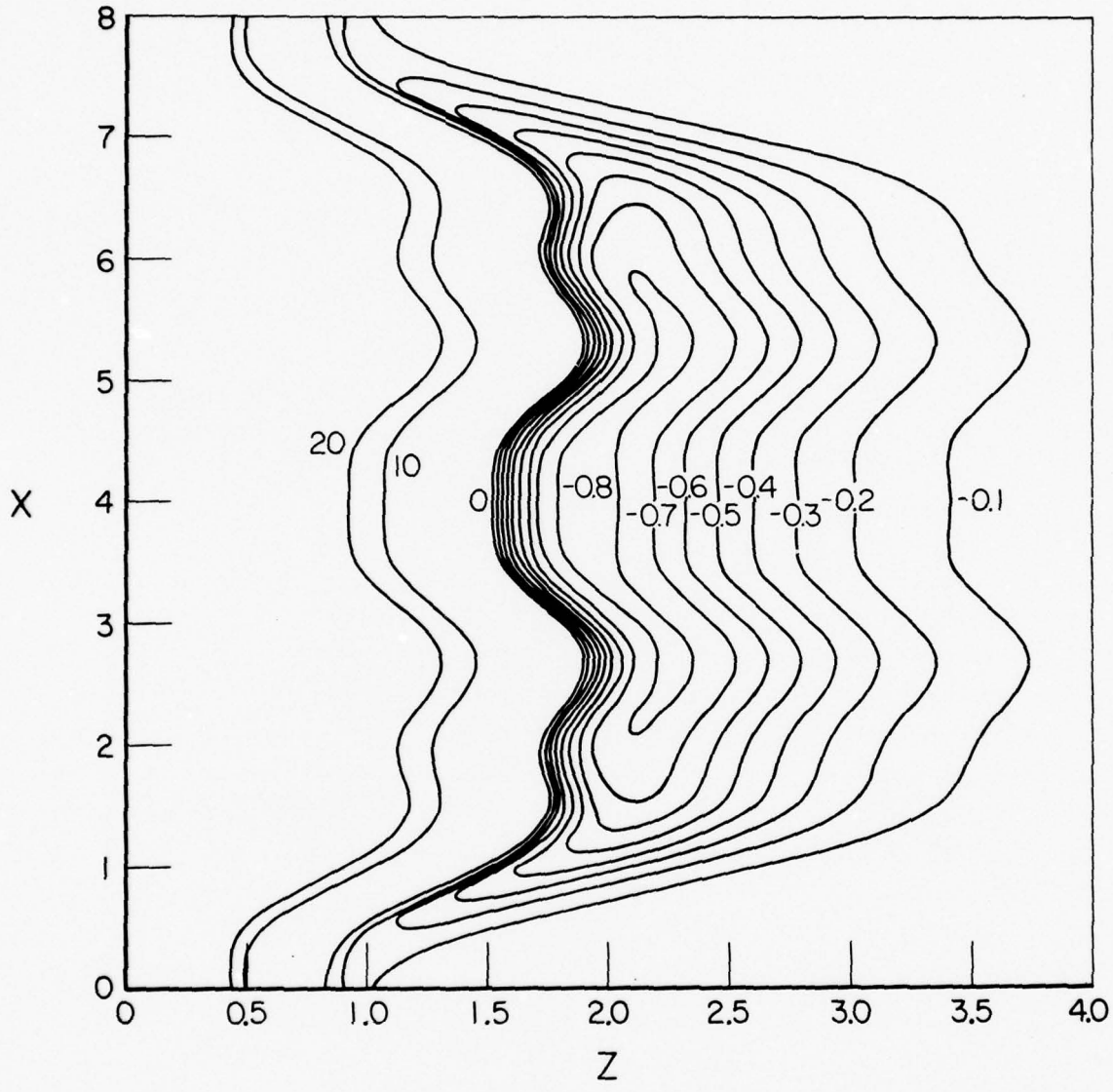

Figure 3a. Equipotential contours (in eV) for an atom approaching surface of graphite in (X,Z) plane as defined in Figure 2 (y=0.0) (a) H atom.

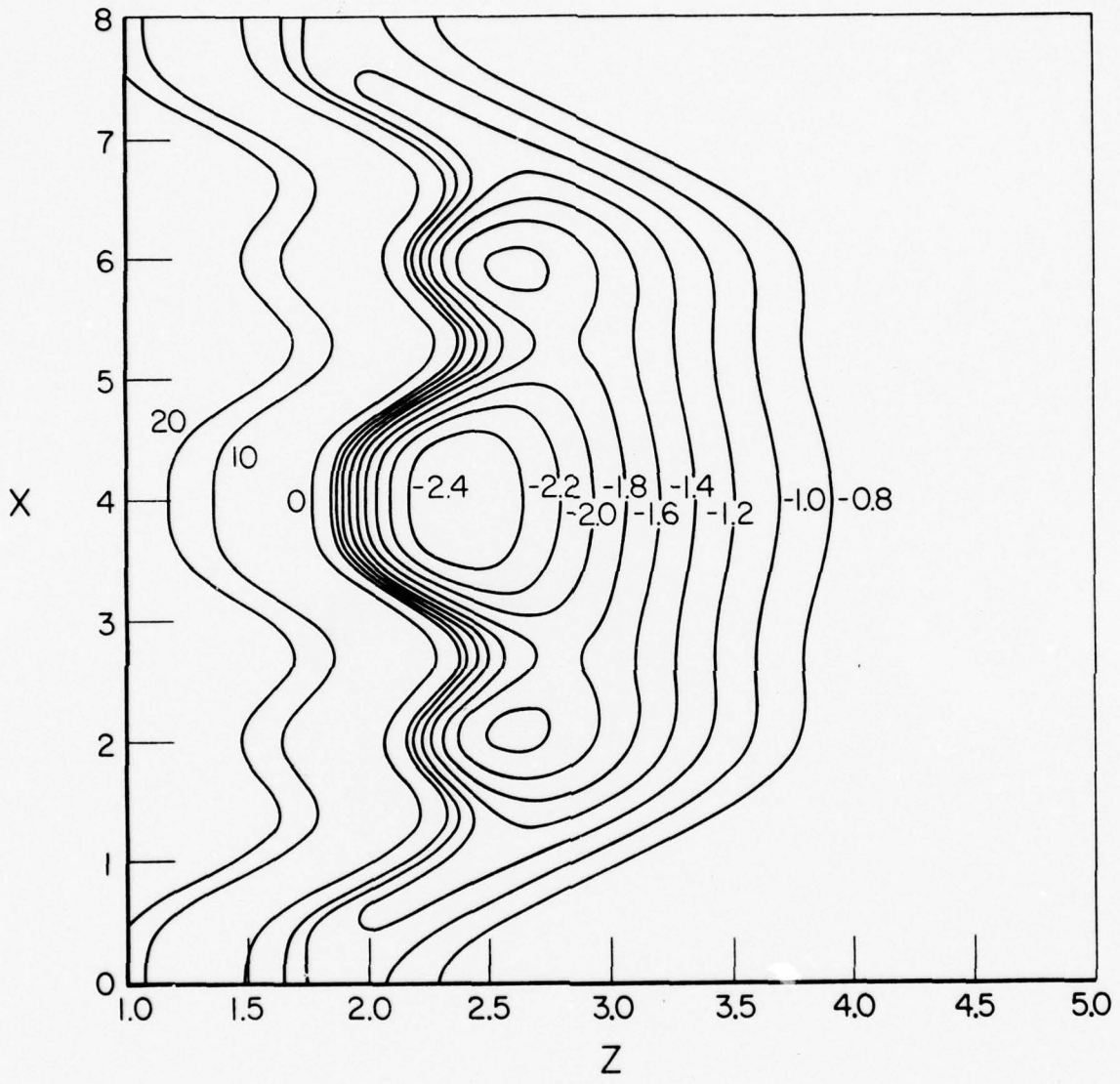

Figure 3b. Equipotential contours (in eV) for an atom approaching surface of graphite in (X,Z) plane as defined in Figure 2 (y=0.0) (b) 0 atom.

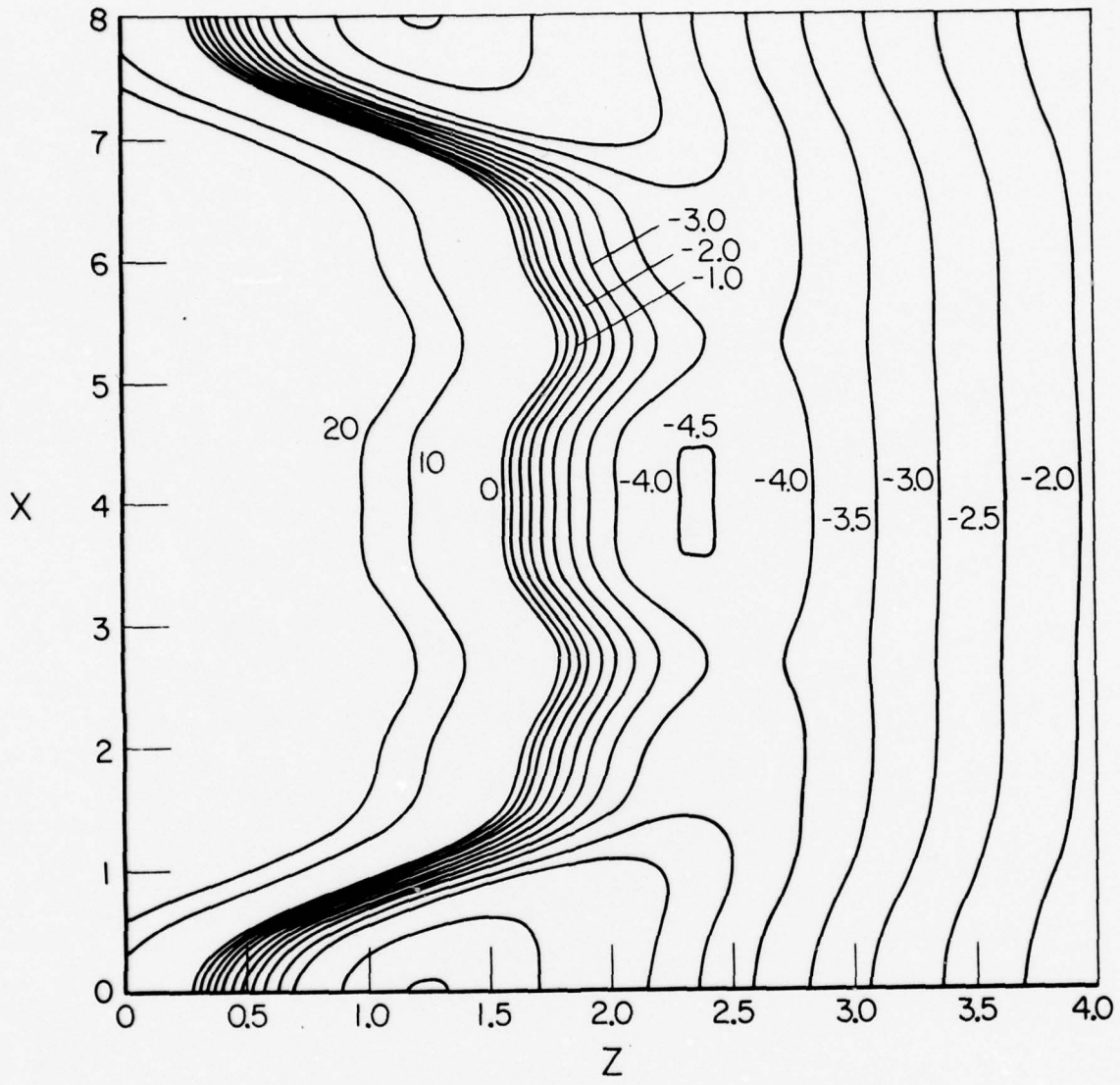

Figure 3c. Equipotential contours (in eV) for an atom approaching surface of graphite in (X,Z) plane as defined in Figure 2 (y=0.0) (c) C atom.

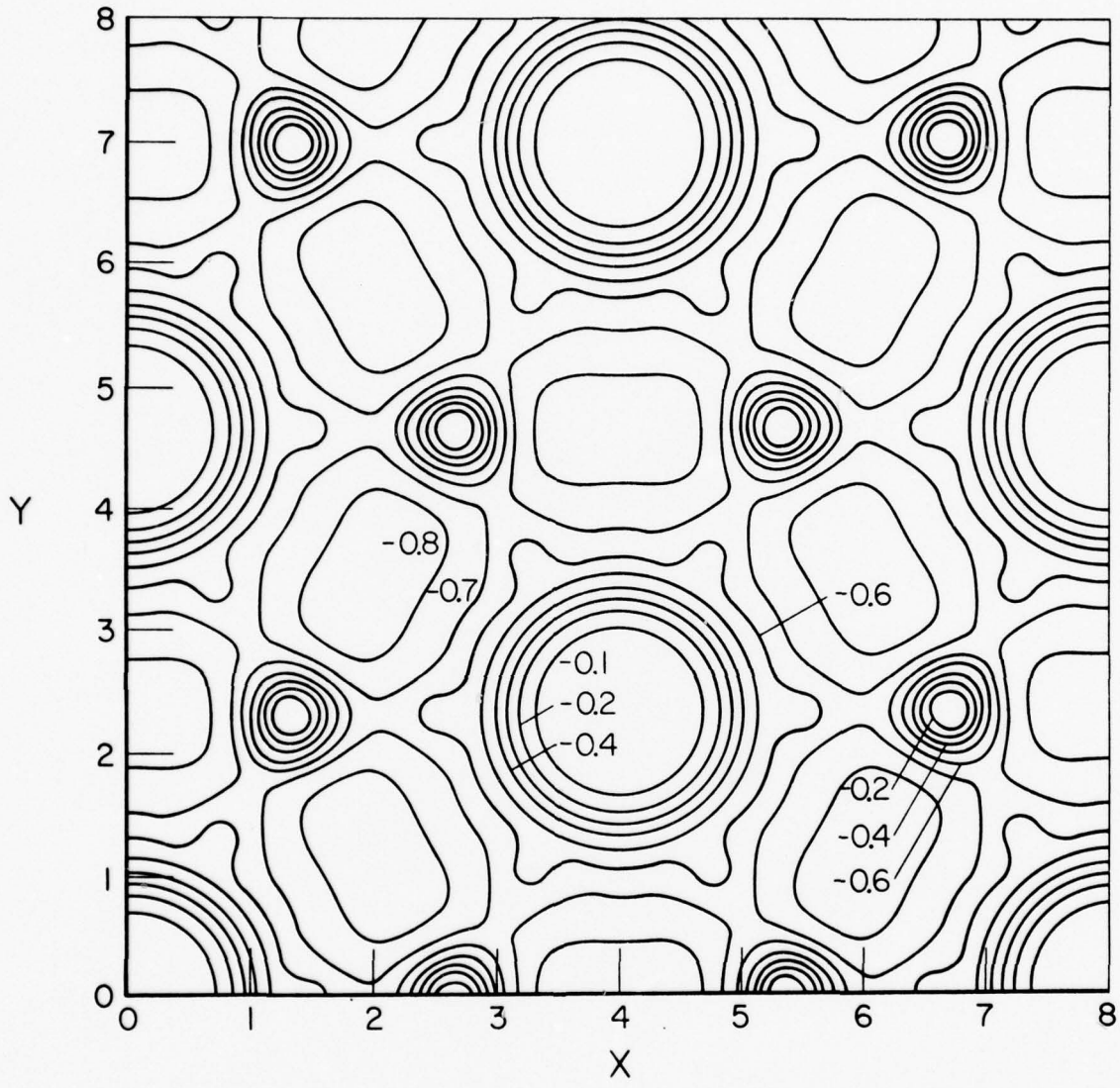

Figure 4a. Equipotential contours (in eV) for an atom in the (X,Y) plane of Figure 2 (a) H (Z=1.9)

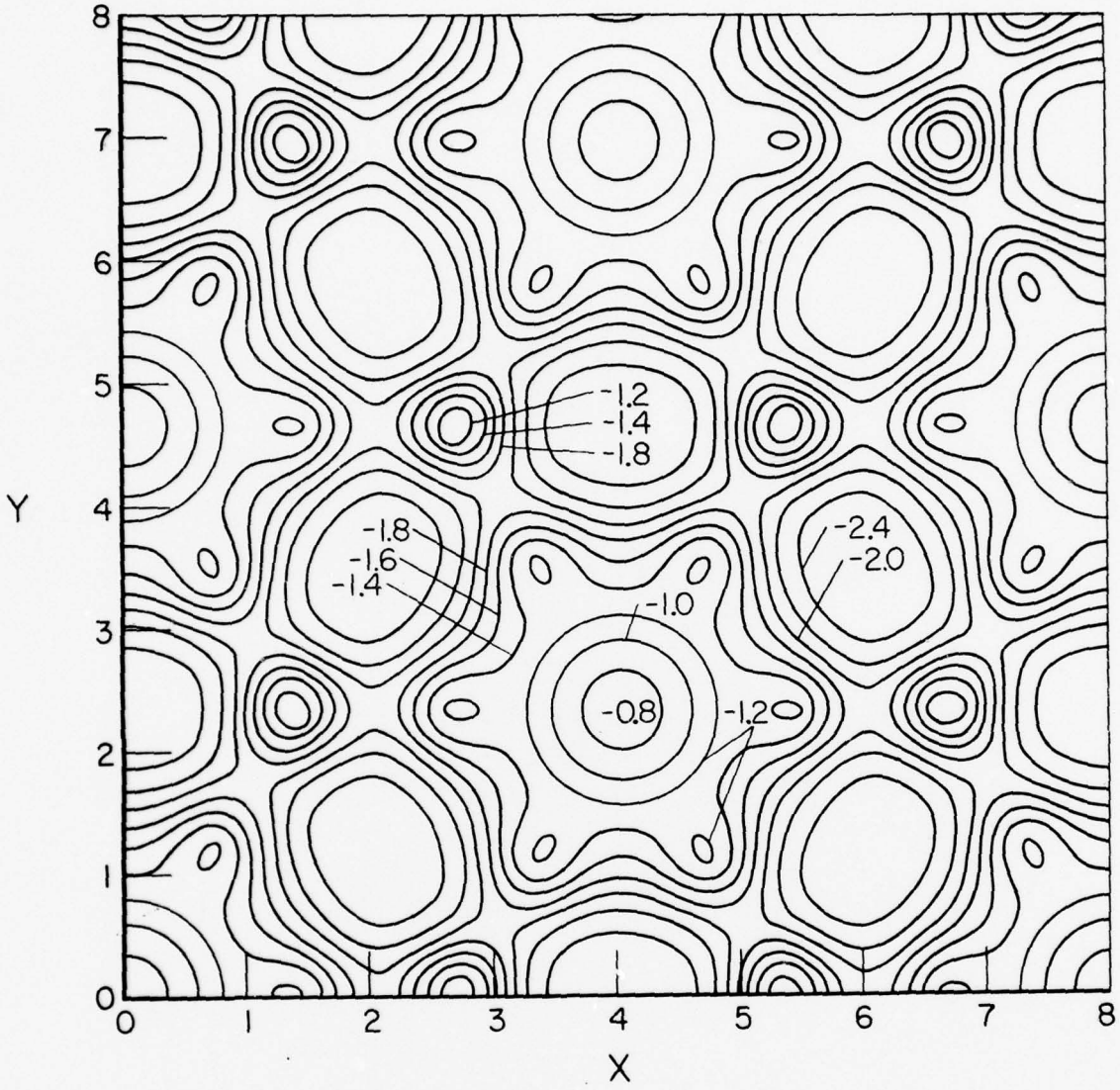

Figure 4b. Equipotential contours (in eV) for an atom in the (X,Y) plane of Figure 2 (b) O (Z=2.4).

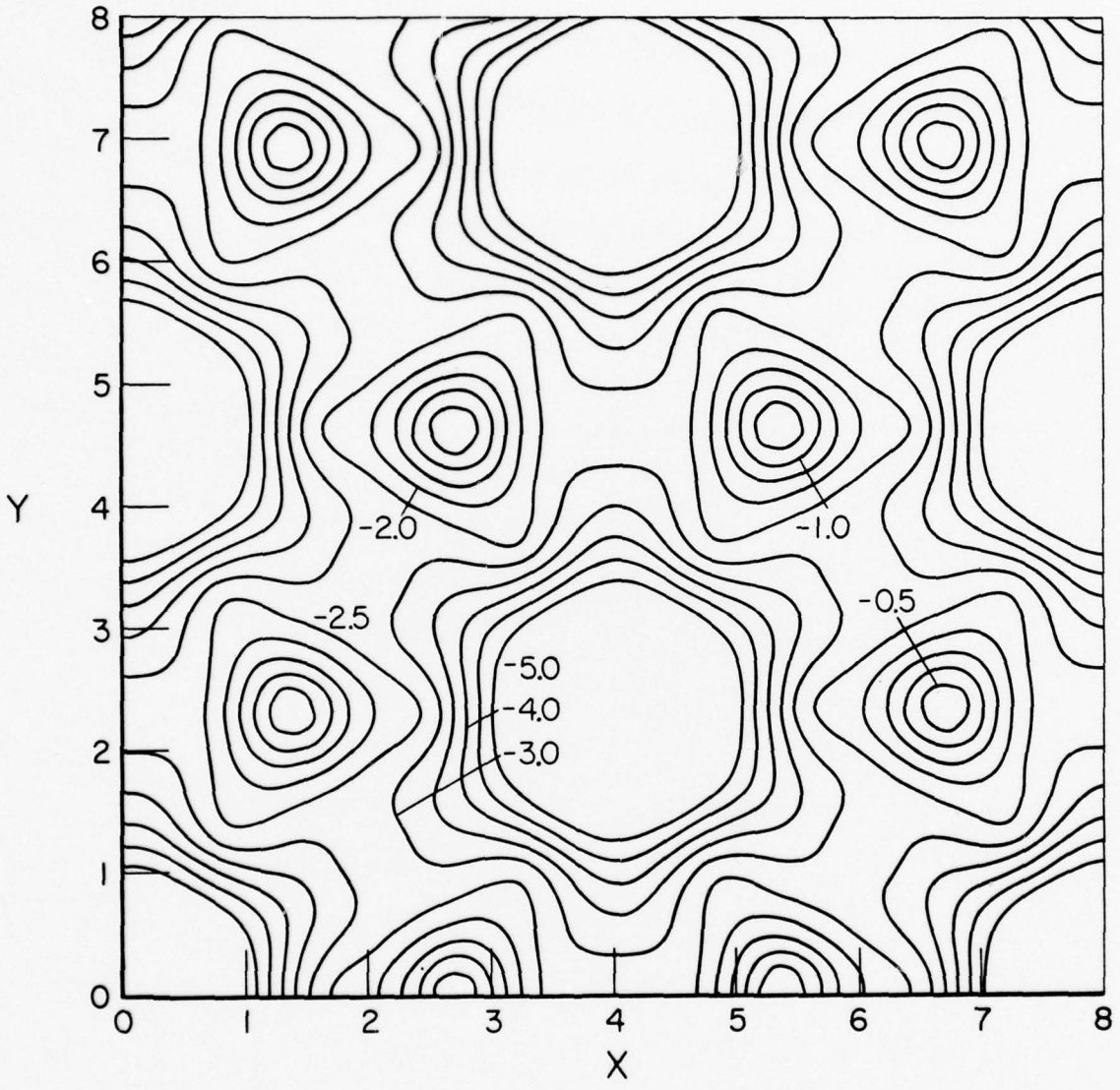

Figure 4c. Equipotential contours (in eV) for an atom in the (X,Y) plane of Figure 2 (C) C (Z=1.8).

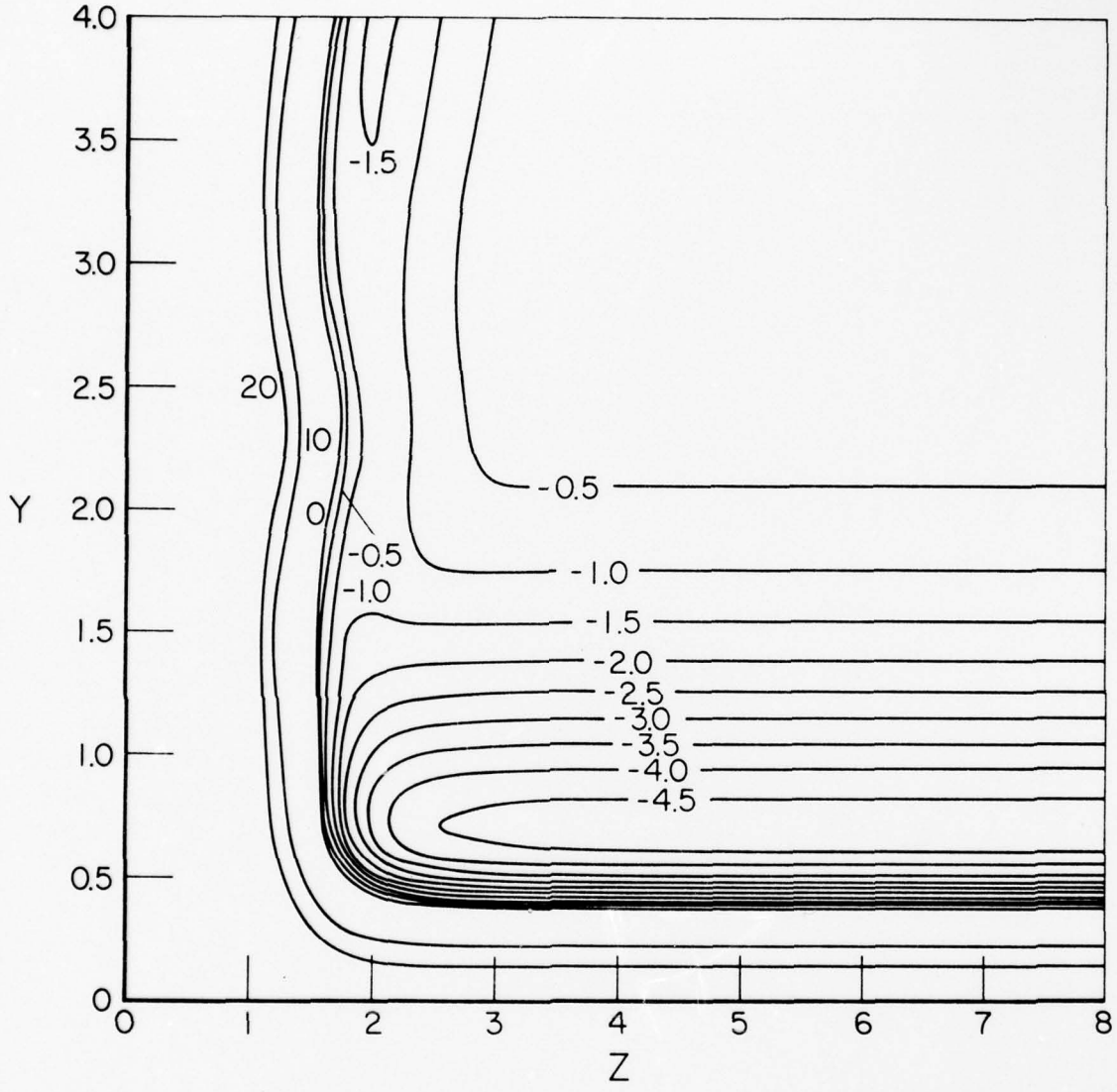

Figure 5a. Equipotential contours (in eV) for H_2 approaching the graphite surface in Figure 2. The H_2 bond is held parallel to the surface and the bond midpoint is fixed over site "A" (7A).

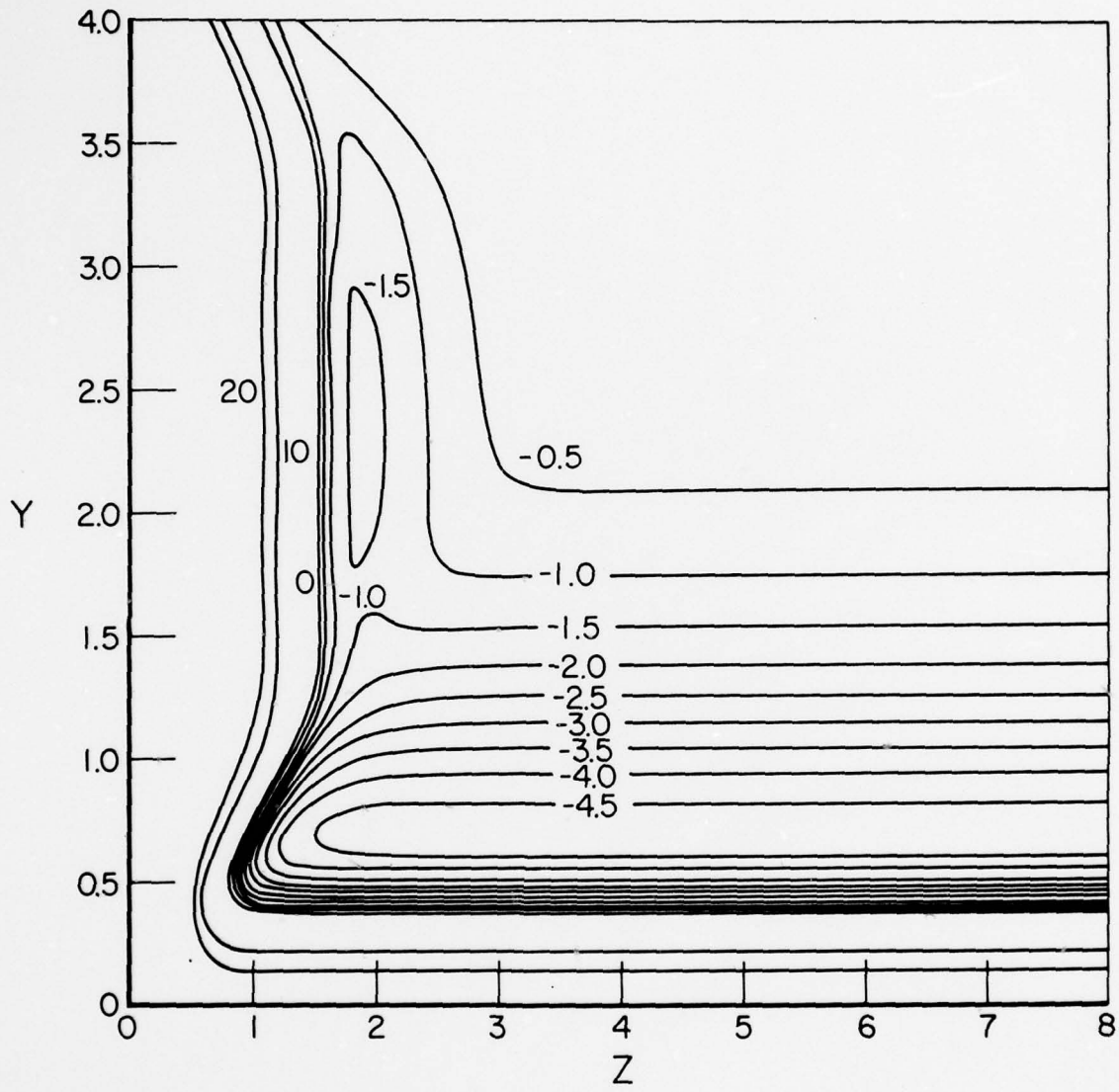

Figure 5b. Equipotential contours (in eV) for H_2 approaching the graphite surface in Figure 2. The H_2 bond is held parallel to the surface and the bond midpoint is fixed over site "B" (7B).

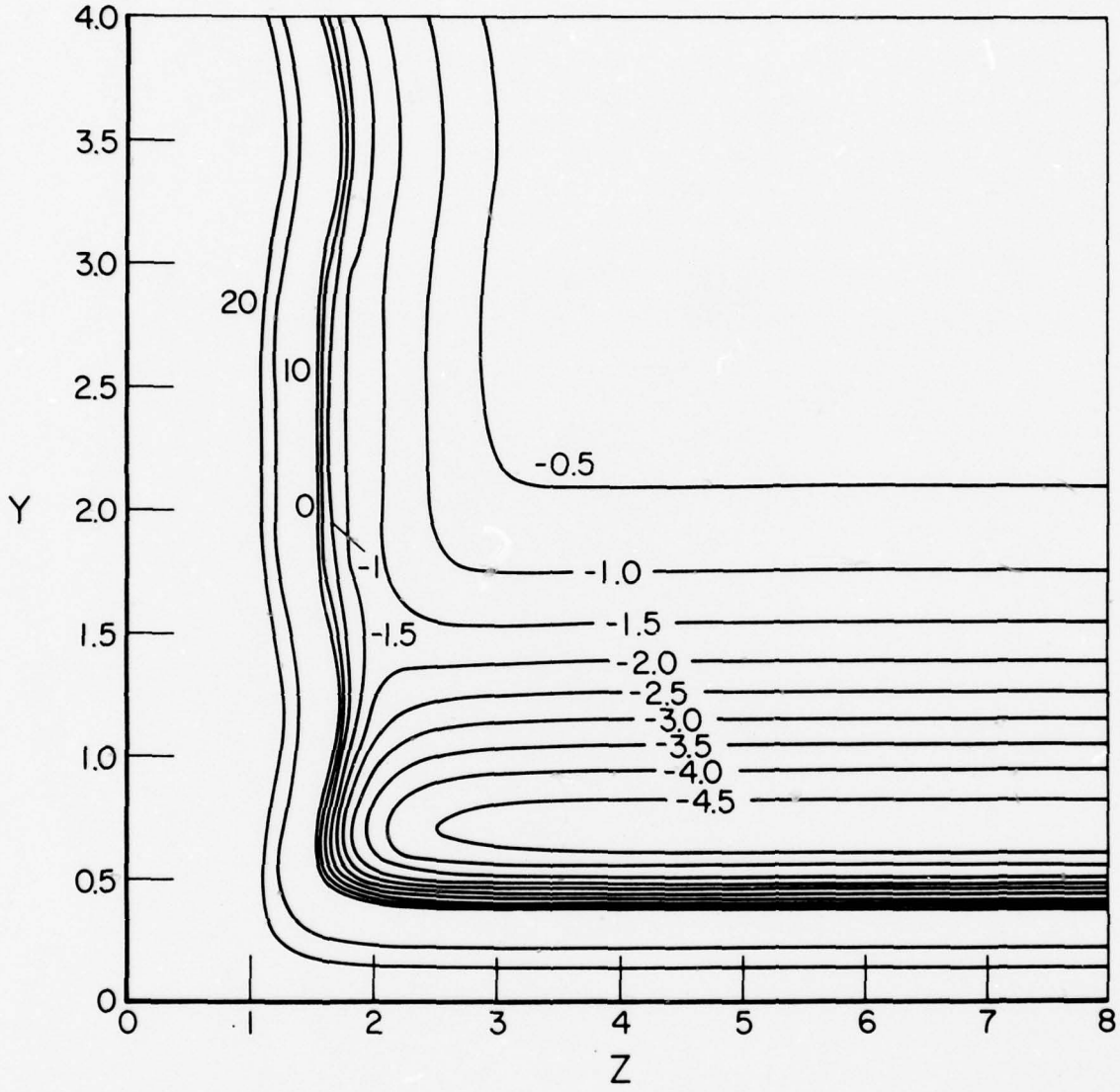

Figure 5c. Equipotential contours (in eV) for H_2 approaching the graphite surface in Figure 2. The H_2 bond is held parallel to the surface and the bond midpoint is fixed over site "C" (7C).

with the surface. Observing the outcome of such trajectories will provide an estimate of the quenching efficiency. The initial conditions for the AB_2 - graphite trajectories are specified as follows. A given trajectory has preselected vibrational quantum numbers (v_1, v_2, v_3), rotational energy, translational energy, direction of approach of the molecule to the surface and temperature of the surface. The initial geometry of the molecule is selected from the inner and outer turning points for the AB bond distances and the angle BAB determined from a normal mode analysis. This gives a total of eight possible geometries for the molecule and each geometry is selected in turn by successive trajectories. A variable vibrational phase is introduced by setting the initial z coordinate of the center of mass of the molecule to be

$$Z_{c.m.} = A + T.V_z. X \qquad (16)$$

where A is a constant (taken to be 10.0 a.u. for CO_2 + graphite trajectories and 8.0 a.u. for H_2O + graphite because of the smaller step size used and therefore longer integration time. V_z is the z component of velocity of the center of mass of the molecule and x is a pseudorandom number between 0 and 1. T is a classical half-period of vibration of the molecule - that of the smallest vibrational frequency (1033.8 a.u. for CO_2 and 432.3 a.u. for H_2O). The velocity of the center of mass is determined by the chosen speed and the direction of approach of the molecule given by angles θ, ϕ in the usual notation. ϕ was chosen to be 0.0 for these calculations. The initial position of the center of masss is determined by Z_{cm}, θ, ϕ and an aiming point on the graphite surface which is the point on the surface that the center of mass of the molecule would pass through if no interaction with the surface were to take place. For the trajectories computed here, the aiming point is chosen to be one of the four sites shown in Figure 2.

The initial orientation of the molecule is specified by the usual Euler angles θ', ϕ', Ψ between 0 and 2π and cos θ' between -1 and 1. The intial velocity of the individual atoms is then determined from the velocity of the center of mass of the molecule, since zero rotational energy was chosen for these calculations.

For the graphite surface atoms that are allowed to move, the initial positions are chosen to be the equilibrium positions of the atoms (at the lattice sites). The Einstein temperature of the graphite surface is

$$\theta^{\text{surface}}_{\text{Einstein}} = \frac{2}{3}\sqrt{0.6}\,\theta^{\text{bulk}}_{\text{Debye}} \tag{17}$$

and

$$\theta^{\text{bulk}}_{\text{Debye}} = 420^{\circ}\text{K}$$

so that

$$\theta^{\text{surface}}_{\text{Einstein}} = 217^{\circ}\text{K} \quad . \tag{18}$$

This leads to a harmonic force constant for the graphite solid atoms of 0.0103 a.u. The initial kinetic energy of each solid atom was chosen equal to the average energy of a harmonic oscillator at the given surface temperature and with an Einstein temperature of 217°K. Kinetic energies of the solid atoms for surface temperatures of 500°K, 1000°K, and 2000°K are given in Table IV.

The step sizes used in the integration procedure were 3.5 a.u. for CO_2 on graphite and 0.7 for H_2O on graphite, the difference being due to the form of potential function used. The functional form used for Δ in the H_2O potential leads to instability of the integration unless the smaller step size is used. To end a trajectory, the usual end conditions for a three atoms-surface trajectory were checked; in addition, a trajectory was considered to be complete if the number of integration steps taken exceeded a given maximum (30,000 steps for CO_2 on graphite and 40,000 steps for H_2O on graphite).

Classical Trajectories: Results

The results of the H_2O and graphite and CO_2 and graphite trajectories are given in Tables V and VI. All of the trajectories we were able to compute resulted in the molecule (or some fragment) remaining bound to the surface. For the H_2O and graphite system, all trajectories resulted in the H_2O molecule being stuck on the graphite surface. H_2O in its (0,0,1) vibrational state was used and the molecule was initially aimed perpendicularly towards an on-top site of graphite; the solid atom in that site was allowed to move. A surface temperature of 500°K was used with H_2O translational energies of 2000°K (10 trajectories) and 1000°K (4 trajectories). Four more trajectories were computed with a graphite

TABLE IV

Graphite surface temperature (°K)	Kinetic energy of surface atoms (a.u.)
500	0.003794
1000	0.008507
2000	0.017989

TABLE V

H_2O + Graphite Trajectories

v_1	v_2	v_3	θ	Aim Point	Surface temperature (°K)	Translational energy (°K)	Number of trajectories	Number of each outcome
0	0	1	0.0	A	500	2000	10	10 a
0	0	1	0.0	A	500	1000	4	4 a
0	0	1	0.0	A	2000	2000	4	4 a

[a] Outcome a corresponds to the H_2O molecule being stuck on the surface.

TABLE VI

CO_2 + Graphite Trajectories

v_1	v_2	v_3	θ	Aim Point	Surface Temperature (°K)	Translational energy (°K)	Number of Trajectories	Number of each outcome
1	0	1	0.0	A	500	2000	4	4b
0	0	1	0.0	A	2000	2000	4	4b
0	0	1	0.0	A	500	1000	4	4b
0	0	1	0.0	A	500	2000	5	5b
0	0	1	15.0	A	500	2000	2	1b, 1c
			30.0				2	2b
			45.0				2	2b
			60.0				2	2b
0	0	1	0.0	B	500	2000	4	3b, 1c
				C			4	4b
				D			4	4b

[b] Outcome b corresponds to an O atom stuck on the surface and a gas-phase CO molecule.

[c] Outcome c corresponds to a gas-phase O atom and CO stuck on the surface.

surface temperature of 2000°K and H_2O translational energy of 2000°K. Each trajectory took about 1000 secs to compute on a CDC 6600, so that it was possible to calculate only a small sample of trajectories for each set of initial conditions. The time taken was to large partly because of the small step size necessary to retain stability in the integration and partly because all these trajectories ended only when the maximum number of steps (40,000) had been taken.

For CO_2 and graphite, the trajectories took somewhat less time to compute (about 250 secs each), both because of the larger step size used and because the majority of trajectories did not take the maximum number of steps but finished when a CO molecule had left the surface, leaving an adsorbed O atom. Trajectories were computed for both the (0,0,1) and the (1,0,1) states of CO_2. Surface temperatures of 500 K and 2000 K were used and CO_2 translational energies of 2000 K and 1000 K. The aiming point on the surface was varied as was the angle of approach O. In all cases except two, the trajectory resulted in an adsorbed O atom and a desorbed CO molecule. In the remaining two cases, the outcome was a gas-phase O atom and an adsorbed CO molecule.

MEASUREMENT OF THE EXTINCTION COEFFICIENT FOR CARBON

The object of this task of the project is to make a simple measurement of the extinction coefficient of carbon particles, at densities appropriate to the shroud concept, in a static matrix of KBr. The matrix material used is a standard spectroscopic matrix, well-characterized and readily available.

To determine the densities required, a simple, 2-core model of the plume, described in Section IV, was adopted. In this model, the plume is assumed to consist first of an inner core of hot gases with base diameter equal to that of the jet exhaust, and with apex pointing rearward. Surrounding this cone is a second cone of the same cone angle, with apex pointing forward, and intersecting the first cone at the edge of the exhaust opening. The particles are assumed to be entrained between these two cones. The particle density for lampblack injected into this volume were calculated and taken as representative.

Lampblack samples obtained from Cabot in Cambridge, Mass., with nominal diameter 1500 Å were used. The lampblack was mixed with KBr powder in the quantities needed and portions of the mixture were pressed into disks for spectroscopic analysis in the 2.6 to 6.0 μm wavelength range. Several disks (5 or 6) were chosen from those fabricated on the basis of total density variation. All densities were required to fall within 10% of the mean.

For an aircraft of velocity 1000 ft/sec. with exhaust diameter of 26.6 inches, the particle density corresponding to an injection rate of R (in oz/sec) is

$$\rho_p = 3.14 \times 10^{-6} R \ (gm/cm^3)$$

The fabricated density was 3.4×10^{-6} (gm/cm^3), corresponding to R = 1.1 oz/sec. Five standard disks with density $\rho_p = 0$ and five with density 3.4×10^{-6} gm/cm^3 were measured, in order to improve the statistics of the measurements. Normalized intensity ratios for each wavelength were obtained by dividing the intensity ratio of the sample average by that of the standard ($\rho_p = 0$) average. The average cross section of a single particle was obtained from

$$\sigma = - \ln(I/I_o)/NT$$

where I/I_o is the normalized intensity ratio, T is the mean sample thickness, and N is the particle density. The values obtained fell in the range $(2.5 - 8.8) \times 10^{-11}$ cm^2/particle, which are comparable in magnitude to published values.[6] The measurements are summarized in Table VII.

Table VII. Analysis of Absorption Measurement Data

(ρ_p = 3.4 x 10^{-6} g/cc, 1.1 oz/sec.)

Wavelength (micrometers)	2.6	3.0	3.5	4.0	4.5	5.0	5.5	6.0
(I/I_o) sample / (I/I_o) standard	.971 (±.029)	.966 (±.026)	.972 (±.025)	.981 (±.023)	.982 (±.024)	.982 (±.019)	.987 (±.021)	.988 (±.018)
10^{11} x σ (cm^2/particle)	2.46 (±1)	8.77 (±7.5)	7.20 (±8.87)	4.86 (±1)	4.62 (±1.3)	4.62 (±1)	3.31 (±1.6)	3.06 (±1.5)

CALCULATION OF SHROUD EFFECT ON SIGNATURE

Plan of Computations

The original plan of this research was to carry out a semiquantitative analysis of the effect of quenching on the shroud effect of carbon particles. Briefly, it was planned to make rough estimates of the mixing layer thickness using data available in the literature. Then, using Air Force data on aircraft velocities, exhaust velocities, temperature profiles and CO_2 and H_2O concentration profiles, the signatures with and without the carbon shroud would be computed using existing radiative transfer programs modified to include the additional effects.

Early in the program, it was pointed out that the Air Force had developed, under contract with General Electric, a comprehensive set of programs for the calculation of jet engine signatures, and that the programs known as SCORPIO III, were installed on the Air Systems Division computer coupler at Wright-Patterson AFB. After some discussion, it was decided to use these programs for the following reasons:

- They were proven programs.
- They could be easily modified.
- They were well documented.
- They included programs for determining the flow field.
- They included all relevant absorption and scattering effects.

Further, the authors of the programs were located nearby and were willing to cooperate in implementing the needed changes. These programs offered a considerable expansion of the sophistication of the signature calculations at no apparent increase in cost to the project. Finally, as discussed below, a later version of the programs, called SCORPIO IIIA, included calculation of the flow field of a carbon shroud and its effect, without quenching, on the IR signature.

There ensued an unfortunate series of events which, ultimately, prevented the use of these programs for the purposes of the project and reduced the available funding to an extend that made it impossible to

return to the original plan. A brief description of these difficulties follows, after which the model calculations, developed to replace the more realistic computations, will be described.

Difficulties With Air Force Codes

After some delays caused by the need for large amounts of permanent file space for the SCORPIO programs, initial attempts were made to run the codes using the test data set installed with the source codes. The data set was not accepted by the code, and one source suggested that SCORPIO III had never been successfully run on the current operating system. When installed the data set would not run, the data set for the test case in the SCORPIO III Users Manual was reconstructed manually. This data set also did not run to completion, and the results that were obtained did not match the results in the Users Manual. At this point it was discovered that the installed code had been modified and that it was an early version of a code known as SCORPIO IIIA, which incorporated shrouding particles. A classified General Electric report describing the SCORPIO IIIA modifications was obtained. Using these modifications together with some of the data changes found in the originally installed test cases, it was possible to obtain a data set that was completely compatible with the installed code. All of these steps were performed laboriously by step-by-step comparison of coded lines, data items, and the various documentations available. When data assembly was completed and run, it was found that the code still did not run to completion because of a coding error. The results that were obtained prior to encountering the coding error, however, now agreed approximately with the test results of the Users Manual when the particle mass injection rate was set to zero. At this point, it appeared that the codes could be made to work, with help from General Electric personnel. However, these efforts had exhausted 80% of the funds allocated for the computations. Further attempts to use the code revelaed several other coding errors which were found and corrected with help from G. E. However, it was never possible to obtain a completely successful run matching all of the output reported in the Users Manual. And, a fatal flaw still remains—the radiation from the hot engine parts does not interact with the plume. This is a major contribution to the signature, and this interaction is essential for operation of the

quenching mechanism. Since the exact cause of and the extent of the correction needed for this problem were not known, it was decided to halt this portion of the program and examine the options available. There appeared to be three viable options, all requiring some additional funding. These were

- Abandon the attempt to use SCORPIO IIIA and return to the original plan to use BCL codes.
- Subcontract the calculations to General Electric to carry out on the latest version of SCORPIO IIIA, installed and routinely run on their computing equipment.
- Abandon large-scale computations and resort to model calculations to give an indication of the relevance of quenching to signature suppression.

Because of limited funding, the third of these options was taken.

The experience with the SCORPIO codes was disappointing, but not entirely wasteful. The completed runs do contain the temperature profiles plume flow data, and exit-plane radiation data necessary to perform quantitative calculations.

Description of the Model

The actual plume situation is modeled as follows: We have a mixture of carbon particles, air, and both excited and unexcited CO_2 molecules. Radiation is incident upon this mixture. The unexcited CO_2 can be excited by the radiation and excited CO_2 can either radiate into the field or can be de-excited without radiation by collision with the carbon particles. Each carbon particle is treated as a sphere of radius a, surrounded by a mixture of air and CO_2 in a spherical region of radius b. The CO_2 molecules can diffuse to the surface, where a fraction γ of them are de-excited. The radius b is chosen to enclose that volume of the air-CO_2 mixture determined by the average density of carbon particles in the plume. At radius b, the excited CO_2 concentration is unchanging, i.e., a pure "reflection" boundary condition is used. The diffusion equation is to be solved for this model to obtain CO_2 concentration profiles as a function of time. The total CO_2 concentration is held constant throughout. CO_2 alone is treated as a radiating species because it is generally regarded as the most important molecule in signature determination.

The use of a diffusion approach in the calculations is motivated by the need to determine the time scale in which the quenching mechanism operates. A short time scale would indicate that the quenching is essentially complete at the exit plane, while a longer time scale would indicate a more gradual rise in the quenching enhancement. A very long time scale would mean that the mechanism is ineffective, since the quenched region would be far behind the aircraft. It is also important to realize that the time scale on which the carbon particles reach equilibrium with the air in the plume (most of the plume gas is nitrogen) is very short. Thus, we can take the carbon particles to have the same temperature and velocity as the air in the slip-stream where mixing is assumed to occur.

Mathematical Description of the Model

The diffusion equation for the model situation is

$$\frac{\partial c^*}{\partial t} = D \frac{\partial^2 c^*}{\partial r^2} + \frac{2D}{r} \frac{\partial c^*}{\partial r} - s_o c^* + Ikc_T \tag{1}$$

where

c^* = Concentration of excited CO_2

c_T = Total concentration of CO_2 = $c^* + c$

D = Diffusion coefficient of CO_2 in N_2 (or Air)

I = Intensity of radiation field

k = cross-section for $c \rightarrow c^*$ transition

$s_o = \lambda + Ik$

λ = net decay rate for $c^* \rightarrow c$

The boundary conditions to be imposed are

$$\frac{\partial c^*(b,t)}{\partial r} = 0 \tag{2}$$

$$\frac{\partial c^*(a,t)}{\partial r} = \frac{1}{4} \frac{\gamma \bar{v}}{D} c^*(a,t) \tag{3}$$

Here

a = radius of carbon particle

b = radius of sphere of influence for one particle

γ = fraction of CO_2^* molecules striking carbon surface which are de-excited without radiation

$\bar{v}$ = average CO_2 molecular velocity.

The derivation of Eq. (1)-(3) follows standard procedures. The initial condition for Eq. (1) is written

$$c^*(r,o) = c_o^* \tag{4}$$

where c_o^* is the concentration of excited CO_2 in the plume at $t = 0$.

The substitution

$$c^*(r,t) = \frac{u(r,t)}{r} + \frac{Ikc_T}{s_o} \tag{5}$$

transforms Eq. (1) into

$$\frac{\partial u}{\partial t} = D \frac{\partial^2 u}{\partial r^2} - s_o u \tag{6}$$

with initial condition

$$u(r,o) = (c^*_o - \frac{Ikc_T}{s_o})r \tag{7}$$

and boundary conditions

$$\frac{\partial u(b,t)}{\partial r} = \frac{1}{b} u(b,t) \tag{8}$$

$$\frac{\partial u(a,t)}{\partial r} = (h + \frac{1}{a})u(a,t) + ha \frac{Ikc_T}{s_o} \tag{9}$$

where

$$h = \frac{1}{4} \frac{\gamma \bar{v}}{D} \tag{10}$$

Our problem has now been reduced to one analogous to heat flow in one dimension through a rod under very general boundary conditions:

1. There is radiation with conductivity s_o along the rod's sides into a medium at u = 0;
2. There is radiation at 4 = b with conductivity 1/b into a medium with u = 0;
3. There is radiation at r = a with conductivity $h + \frac{1}{a}$ into a medium with

$$u = \frac{ha^2}{1 + ha} \frac{Ikc_T}{s_o} .$$

We follow standard methods to obtain a solution. First, we put

$$u(r,t) = v(r) + w(r,t) \tag{11}$$

Then we can obtain the two differential equations

$$D \frac{\partial^2 v}{\partial r^2} - s_o v = 0 \tag{12}$$

with

$$\frac{\partial v(b)}{\partial r} = \frac{1}{b} v(b) \tag{13}$$

$$\frac{\partial v(a)}{\partial r} = (h + \frac{1}{a}) v(a) + ha \frac{Ikc_T}{s_o} \tag{14}$$

and

$$\frac{\partial w}{\partial t} = D \frac{\partial^2 w}{\partial r^2} - s_o w \tag{15}$$

with

$$w(r,0) = r(c_o^* - \frac{Ikc_T}{s_o}) - v(r) \tag{16}$$

$$\frac{\partial w(b,t)}{\partial r} = \frac{1}{b} w(b,t) \tag{17}$$

$$\frac{\partial w(a,t)}{\partial r} = (h + \frac{1}{a}) w(a,t) \tag{18}$$

This technique gives us a simple time-independent equation for v satisfying the full boundary conditions and a time dependent equation for w satisfying a set of simpler, homogeneous, boundary conditions.

The solution of the v(r) equations are easily obtained by Laplace transformation methods and is

$$v(r) = -\frac{haIkc_T}{s_o}\left[\frac{\cosh\mu_o(b-r) - \frac{1}{\mu_o b}\sinh\mu_o(b-r)}{(h+\frac{1}{a}-\frac{1}{b})\cosh\mu_o\ell - [\frac{h+\frac{1}{a}}{b\mu_o} - \mu_o]\sinh\mu_o\ell}\right] \tag{19}$$

where

$$\mu_o = \sqrt{\frac{s_o}{D}} \quad ; \quad \ell = b-a \tag{20}$$

The w(r,t) equations are straightforward to solve by variable separation. Put

$$w(r,t) = R(r)T(t) \tag{21}$$

Then, we find

$$T(t) + T_o e^{-\alpha t} \tag{22}$$

$$R(r) = A\cos\mu r + B\sin\mu r \tag{23}$$

where α is a separation constant and

$$\mu = \sqrt{\frac{\alpha - s_o}{D}} \tag{24}$$

The boundary conditions, Eq. (17) and (18), lead to a consistency condition:

$$\tan\mu\ell = \frac{\mu(h+\frac{1}{a}-\frac{1}{b})}{\mu^2 + \frac{1}{b}(h+\frac{1}{a})} \tag{25}$$

which has real, discrete eigenvalues μ_n. Using either of the boundary conditions allows R(r) to be written as

$$R_n(r) \propto X_n(r) \tag{26}$$

where

$$X_n(r) = N_n[\cos\mu_n(b-r) - \frac{1}{b\mu_n}\sin\mu_n(b-r)] \tag{27}$$

and N_n is a normalization factor. Thus, the general solution can be written

$$w(r,t) = \sum_{n=1}^{\infty} A_n X_n(r) e^{-(s_o + D\mu^2_n t)} \tag{28}$$

Only positive eigenvalues are used because of symmetry. There is no eigenvalue for $n = 0$ as long as $h \neq 0$. The A_n are found from the initial condition:

$$w(r,o) = r(c_o^* - \frac{Ikc_T}{s_o}) - v(r) = \sum_{n=1}^{\infty} A_n X_n(r) \tag{29}$$

The X_n are orthogonal, so we find

$$A_n = \int_a^b [(c_o^* - \frac{Ikc_T}{s_o} r - v(r)] X_n(r) dr \tag{30}$$

The time scale of the evolution of c^* is determined by the lowest eigenvalue, μ_1, and we define the time constant of the system to be

$$\tau_1 = \frac{1}{s_o + D\mu_1^2} \tag{31}$$

To determine μ_1, we have to solve the eigenvalue equation, Eq. (25). Define

$$\begin{aligned} \zeta &= \mu\ell \\ \varepsilon &= \frac{a}{b} < 1 \\ \rho &= 1 + ha > 1 \end{aligned} \tag{32}$$

Then Eq. (25) can be written as

$$\tan\zeta = \frac{(1-\varepsilon)(\rho-\varepsilon)\zeta}{\zeta^2\varepsilon + (1-\varepsilon)^2\rho} \tag{33}$$

Generally, we expect b>>a, so $\varepsilon<<1$. Then we can rewrite (33) as

$$\cot\zeta = \frac{\varepsilon}{\rho}\zeta + \frac{1}{\zeta} \tag{34}$$

and we have a one-parameter set of eigenvalues to examine. Since $\frac{\varepsilon}{\rho}$ is small, the solutions will lie near the solution of

$$\cot\zeta = 1/\zeta \text{ or } \tan\zeta = \zeta \tag{35}$$

These solutions are tabulated.[7] We find $\zeta_1 \sim 4.5$ so

$$\mu_1 \sim \frac{4.5}{\ell} \tag{36}$$

The time constant can now be written as

$$\tau_1 = \frac{\ell^2}{s_o\ell^2 + (4.5\ D)^2} \tag{37}$$

For small $s_o\ell^2$, using $D \sim 0.5$ cm^2/sec for typical plume temperature and pressure, we estimate $\tau_1 = 10^{-4}$ sec for ℓ = 1 mm and $\tau_1 = 10^{-8}$ sec for ℓ = 1 μm. If $s_o\ell^2$ is large, then $\tau = s_o^{-1}$, independent of the value of ℓ. We will see below that $s_o\ell^2$ is small for our system.

Signature Calculations

Having obtained solutions to the diffusion equation, we are in a position to set up the formulae for the calculation of IR signatures. It is not intended that such calculations be complete, but only that some useful estimate of the enhancement of absorption by quenching be obtained. The inputs from the diffusion equation solutions are the concentrations,

c and c^*. The first step in a signature calculation is to calculate the concentrations, $\bar{c}$ and $\bar{c}^*$, averaged over the volume b. We define this average by

$$\bar{c}^*(t) = \frac{3}{b^3} \int_a^b c^*(r,t) r^2 dr \tag{38}$$

i.e., the volume average over the characteristic volume. This average, combined with the exhaust flow rate and the air speed of the aircraft, determines a variation of concentration, from exit plane backwards into the distant plume, arising from the time dependence of c^*. That is, as we move back from the exit plane, we pass to concentration corresponding to later time epochs in the solution of the diffusion equation.

The next step would normally be to set up some model for the plume structure, and carry out numerical calculations of the signature for various aspect angles. Alternatively, we can simply calculate the total extinction coefficient for a representative situation. This enables us to reduce our assumptions about the plume to the bare minimum and to carry out a semi-analytic analysis. We assume that the plume consists basically of two parts, a central hot core and a flaring-out region of cooler gases (see Fig. 6). The cone angle of both regions are taken to be the same. Then,

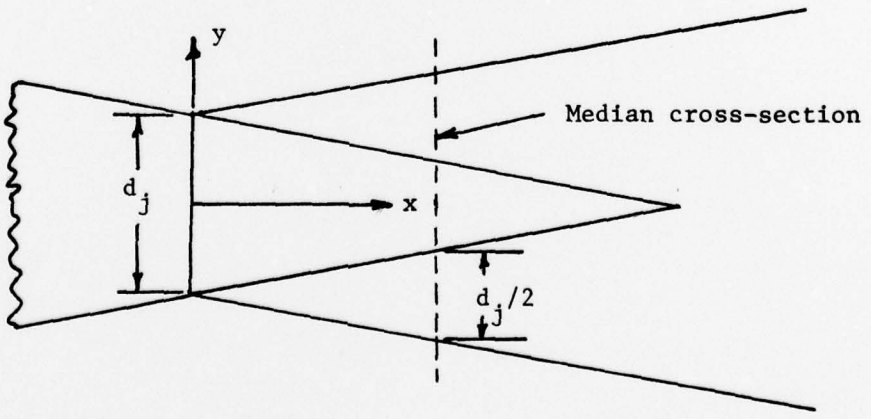

Fig. 6. Schematic of plume-shape assumption.

we assume the particles are mixed into the cool-gas region. The median thickness of this region and the mean radius of the median annular cross-section are both equal to $\frac{1}{2} d_j$. If v is the aircraft velocity, then new volume is swept out at the rate

$$\dot{V} = \frac{1}{2} \pi d_j^2 v \tag{39}$$

If particles are injected at the rate of R oz/sec, then the particle mass density in the shroud is

$$\rho_p = R/\dot{V} = (\frac{a}{b})^3 \rho_c \quad , \tag{40}$$

since the radius of a particle is a and each particle has an associated volume corresponding to a sphere of radius b. In (40), ρ_c is the density of graphite, $\rho_c = 2.25$ gm/cm^3. Using the data from Table VIII, we obtain from Eq. (39) and (40)

$$b/a = 104/R^{1/3} \tag{41}$$

In order to cover the practical range of commercially available lampblacks and injection rates that are reasonable, we consider the values

$a = 500, 1000, 5000, 10{,}000$ Å

$R = 1, 10, 100$ oz/sec.

To determine the time evolution of the quenching effect, we use the values from Table VIII to get IR = 0.213/sec. Thus, since $\lambda = 500$/sec, s_o is dominated by λ. However, s_o^2 is still small compared to $(4.5\ D)^2$ in Eq. (37). Values of τ_1 are given (in microseconds) in Table IX. For v = 1000 ft/sec, the quenching effect is essentially complete for distances larger than about 1 cm behind the exit plane. Hence, diffusion does not appear to create any significant slowing of the quenching mechanism.

The next step is to examine the effective total extinction coefficient. Light passing through the shroud is attenuated both by absorption on the lampblack particles and by absorption through excitation of the un-excited CO_2 molecules. The carbon contributes a term

Table VIII. Data Values Used in Calculations

From SCORPIO III Codes:

d_j = 26.6 in = 67.6 cm

V = 1000 ft/sec. = 3.1×10^4 cm/sec

P = 0.45 Atm.

T = 1230°R = 328°K

at $x_o = d_j$, $\gamma_o = \frac{1}{2} d_j$

Radiant Intensity = 40 Watts/steradian

$I_o = 7 \times 10^{-3}$ Watts/cm^2 = 1.5×10^{17} photons/sec

(at x_o, γ_o and 4.3 μm wavelength band)

$c_T = 5 \times 10^{16}$ molecules of CO_2/cm^3

From literature and direct calculation:

$\lambda = 500\ sec^{-1}$

$k = 1.4 \times 10^{-18}$ cm^2/molecule

D for CO_2 in N_2 = 0.165 cm^2/sec

AT P,T above, D = 0.43 cm^2/sec

ρ_c = density fo Carbon = 2.25 gm/cm^3

$\bar{v}$ = thermal velocity for CO_2 molecule at 328°K

= 3.81×10^4 cm/sec.

$$\alpha_c = \sigma_c \times \text{concentration of carbon particles}$$

$$= \sigma_c / (\frac{4}{3} \pi b^3) = 0.239 \frac{\sigma c}{b^3} \tag{42}$$

to the extinction coefficient. Using the largest measured value from the third section of this report, we find

$$\alpha_c = 2.1 \times 10^{-11} b^{-3} (cm^{-1}) \tag{43}$$

Values of α_c are listed in Table IX.

The contribution from unexcited CO_2 is obtained by calculating the long-time, mean concentration of unexcited CO_2 in the plume. To do this, we need to know the intensity throughout the thickness of the shroud. Examination of the long-time solution, from Eq. (5), (11), and (28)

$$c^*(r,\infty) = \frac{Ikc_T}{s_o} + v(r)/r \tag{44}$$

with v(r) given in Eq. (19), shows that c^* is a nonlinear function of I. However, since λ is the dominant factor in s_o, this nonlinearity is effectively eliminated.

The long-time behavior of c^* is strongly dependent on the parameter μ_o, given in Eq. (2). For the parameter values of significance to us, we have

$$\mu_o = \sqrt{\frac{s_o}{D}} = 34.1 \text{ cm}^{-1}$$

The arguments of the hyperbolic functions are at most $\mu_o b$ in magnitude. Referring to Table VIII, we see that the largest value of $\mu_o b$ is 0.355, occurring for a = 1 μm, R = 1 oz/sec. Considering the smallness of the $\mu_o b$, expansion of the expression for c^* in powers of $\mu_o b$ appears to be one way to simplify the analysis. The interrelationship among the parameters in the full expression, is very delicate, so we must proceed cautiously. c^* is given by

Table IX. System Parameters and Calculated Results

a μm	b μm	τ_1 μ sec	$\mu_o b$	α_c (cm^{-1})	$\bar{N}/_D$	P_{max}
			R = 1 oz/sec:			
0.05	5.20	0.071	0.0177	0.149	0.882	0.414
0.10	10.4	0.283	0.0356	0.0187	0.776	2.91
0.50	52.0	7.06	0.177	1.49×10^{-4}	0.303	142.1
1.00	104.0	27.9	0.354	1.87×10^{-5}	0.131	492.4
			R = 10 oz/sec:			
0.05	2.42	0.0149	8.21×10^{-3}	1.49	0.987	0.0464
0.10	4.83	0.060	0.0164	0.186	0.972	0.365
0.50	24.2	1.49	0.0821	1.49×10^{-3}	0.813	3.817
1.00	48.3	5.96	0.164	1.86×10^{-4}	0.598	224.8
			R = 100 oz/sec:			
0.05	1.12	3.1×10^{-3}	3.81×10^{-3}	14.9	0.999	4.70×10^{-3}
0.10	2.24	0.0122	7.63×10^{-3}	1.86	0.997	0.0376
0.50	11.2	0.307	0.0381	0.0149	0.977	4.60
1.00	22.4	1.23	0.0763	1.86×10^{-3}	0.937	35.3

$$\frac{c^*(r_1 o)-c^*(r_1 h)}{c^*(r_1 o)} = \frac{a}{r}(ha)\ \frac{\cosh\mu_o(b-r)-\frac{1}{\mu_o b}\sinh\mu_o(b-r)}{(1+ha-\frac{a}{b})\cosh\mu_o\ell\ -\frac{1}{\mu_o b}(1+ha-\frac{a}{b}(\mu_o b)^2)\sinh\mu_o\ell} \tag{47}$$

where

$$c^*(r,o) = \frac{Ikc_T}{s_o} \tag{48}$$

and h is given by Eq. (10). Using = 0.8 and $\bar{v}$, D from Table VIII, we find h = 1.77 x 10^4 cm^{-1}. For $_o b = 0$, the right-hand side of (47) is unity, indicating that $c^*(r,h) = 0$ in this limit. This means that the average concentration of unexcited CO_2 molecules is, according to Eq. (38)

$$\bar{c} = [1 - (\frac{a}{b})^3]\ c_T \tag{49}$$

where the factor in square brackets simply reflects the space occupied by the particles, and can be taken as unity for the range of a and b of interest to us.

The expansion through terms of second order in $\mu_o b$ is expressed as a rational function, N/D, with

$$N = \frac{a}{b}\ (ha) + \frac{1}{2}\frac{a}{r}\ (ha)\ \frac{2+\frac{r}{b}}{3}\ (1-\frac{r}{b})^2(\mu_o b)^2 \tag{50}$$

$$D = \frac{a}{b}\ (ha) + \frac{1}{2}\ (\frac{\ell}{b})^2\ \{\frac{2a}{\ell} + \frac{2+\frac{a}{b}}{3}\ (1+ha)\ -3\ \frac{a}{b}\}\ (\mu_o b)^2 \tag{51}$$

Further expansion is not advisable because the leading term in both expressions is rather small. The numerator expression is to be averaged according to Eq. (38):

$$\bar{N} = [1 - (\frac{a}{b})^3]\ \frac{a}{b}(ha) + \frac{1}{2}\frac{a}{b}(ha)(\mu_o b)^2\ \{(\frac{a}{b})^2 - (\frac{a}{b})^3 - (\frac{a}{b})^5 + \frac{1}{5}\} \tag{52}$$

For our purposes, we can set $\frac{a}{b}<<1$, $\ell \simeq b$ at this stage. Then

$$\bar{N} \simeq \frac{a}{b}(ha)\ [1 + \frac{1}{10}\ (ha)(\mu_o b)^2] \tag{53}$$

$$D \simeq \frac{a}{b}(ha) + \frac{1}{3}(1 + ha)(\mu_o b)^2 \tag{54}$$

In Table VIII we calculate $\bar{N}/D$ for our parameters. For small particles or large R, the quenching is nearly complete.

To estimate the effect of the quenching mechanism, we need to know the fraction, f^*, of excited CO_2 in the plume region. This number is not readily available, and its estimation involves solution of non-equilibrium processes. The ratio $\bar{N}/D$, calculated above, gives us the fraction of excited CO_2 molecules that are de-excited by quenching, based on an equilibrium calculation. The excited fraction for this case is (refer to Table VIII)

$$f^*_{eq} = {}^{Ik}/_{s_o} \simeq {}^{IK}/_{\lambda} = 4.2 \times 10^{-4}$$

which is a lower limit. In this limit, it is clear that the mechanism plays a negligible role. The nonequilibrium processes in the engine combustion and plume formation will raise f^* from this value. The change in extinction coefficient due to quenching can be written as

$$\Delta\alpha_{co_2} = \left(\frac{\bar{N}}{D}\right) f^* \, c_T k \tag{55}$$

whereas, for h = 0, we will have the contribution

$$\alpha_{co_2}\Big|_{h=0} = (1 - f^*) c_T k \tag{56}$$

Thus, the fractional change in extinction coefficient is

$$p = \frac{\Delta\alpha_{co_2}}{\alpha_c + \alpha_{co_2}|_{h=0}} = \frac{\left(\frac{\bar{N}}{D}\right)_{f^*} c_T k}{\alpha_c + (1 - f^*) c_T k} \tag{57}$$

with α_c given in Eq. (43). The largest values of this ratio are found for $f^* = 1$, when

$$p_{max} = \frac{c_T k}{\alpha_c} \left(\frac{\bar{N}}{D}\right) \tag{58}$$

From Table VIII,

$$c_T = 5.0 \times 10^{16} \text{ molecules/cm}^3$$

so $c_T k = 0.07$. In Table IX, are given values of α_c and p_{max}, for the parameter ranges of interest. It should be emphasized that the equilibrium value of f^* leads to a negligible effect, as mentioned above, even when α_c is very small, because the limit of Eq. (57) then becomes

$$\lim_{\alpha_c \to 0} p = \frac{\bar{N}}{D} \frac{f^*}{1-g} \sim f^* \frac{\bar{N}}{D} \tag{59}$$

which is smaller than f^*.

Concluding Remarks

The results of the last section indicate that under certain conditions, and in certain regions of the (a,R) parameter space, the quenching effect can be significant. The maximum possible enhancement occurs for the largest values of a and the smallest values of R. However, for this enhancement to be meaningful, the nonequilibrium processes must cause most of the CO_2 exiting the jet engine to be excited. In the simple models used here, the influence of nonequilibrium processes is reflected in a reduction in the value of λ appropriate for the calculations. The value, $\lambda = 500 \text{ sec}^{-1}$, was determined by using the measured band strength of the v_3 (4.3 μm) line of CO_2, and, from this, finding the Einstein "A coefficient". This gives the probability/second of spontaneous emission from an excited CO_2 molecule in equilibrium with its radiation field. Collisions are not explicitly included in A, and if these and other nonequilibrium processes result in a higher concentration of CO_2^*, this will be reflected in a smaller effective value for A (i.e., λ).

The degree of excitation required in our model for useful quenching is quite high. The location of our typical plume data, taken from SCORPIO III, is about one exhaust diameter back and one-half of an exhauster diameter out radially. At this point, the gas has already cooled to 328°K. Unless highly nonequilibrium conditions exist it does not, therefore, appear reasonable to expect a very high excitation of CO_2, but for the larger values of a, the absorption from carbon is so reduced that even the enhancement from an only-moderately-excited gas will be a great improvement - perhaps a factor of 50-100 in α_{TOTAL}. For the smaller particle sizes, the quenching enhancement is negligible for all R. For high injection rates, only a small multiplier may be introduced by quenching effects, and except for the largest a, this is not significant. We therefore conclude that quenching is not an effective enhancement mechanism except in very special cases, namely, for large a.

References

1. S. J. Berstein, "The Successful Testing of an Operationally Feasible System for Infrared Suppression - Pave Shield" (U), Air Force Cambridge Research Labs, Hanscom AFB, Mass., AFCRL-TR-76-0007, Final Report, Jan. 6, 1976, 32 pp. (Report Secret)

2. J. H. McCreery and G. Wolken, Jr., J. Chem. Phys. 66, 2316 (1977).

3. J. H. McCreery and G. Wolken, Jr., J. Chem. Phys. 67, 2551 (1977).

4. H. J. Bennett, B. McCarroll, R. P. Messmer, Surf. Sci. 24, 191 (1971).

5. M. R. Hayns, Theoret. Chim. Acta (Berlin) 39, 61 (1975).

6. C. L. Tien, D. G. Doornink, and D. A. Rafferty, "Attenuation of Visible Radiation by Carbon Smokes", Combustion Science and Technology 6, 55-59 (1972).

7. M. Abramowitz and I. A. Stegun, Handbook of Mathematical Functions, National Bureau of Standards AMS55, U.S. Government Printing Office, (1964) p. 224.

REPORT DOCUMENTATION PAGE

BEFORE COMPLETING FORM

1. REPORT NUMBER (18) AFOSR-TR-79-0009 (19)	2. GOVT ACCESSION NO. / 3. RECIPIENT'S CATALOG NUMBER: 6 6794
4. TITLE (and Subtitle): (6) Analysis of a Model for IR Suppression (U)	5. TYPE OF REPORT & PERIOD COVERED: Final Report. April 1, 1977-July 31, 1978
	6. PERFORMING ORG. REPORT NUMBER: (9) Final rept. 1 Apr 77-31 Jul 78,
7. AUTHOR(s): (10) R. P. Kenan, G. Wolken, J. McCreery, R. Barnes, D. Applebaum ~~and C. Whitacre~~	8. CONTRACT OR GRANT NUMBER(s): (15) F49620-77-C-0056
9. PERFORMING ORGANIZATION NAME AND ADDRESS: Battelle Columbus Laboratories, 505 King Avenue, Columbus, Ohio 43201	10. PROGRAM ELEMENT, PROJECT, TASK AREA & WORK UNIT NUMBERS: 61102F (16) 2301 A5 (17)
11. CONTROLLING OFFICE NAME AND ADDRESS: Air Force Office of Scientific Research, Attn: NP, Building 410, Bolling AFB, Washington, D.C. 20332	12. REPORT DATE: (11) 29 Sep 78 ~~September 29, 1978~~
	13. NUMBER OF PAGES: 50 (12) 55 p.
14. MONITORING AGENCY NAME & ADDRESS (if different from Controlling Office)	15. SECURITY CLASS. (of this report): Unclassified
	15a. DECLASSIFICATION/DOWNGRADING SCHEDULE: N.A.

16. DISTRIBUTION STATEMENT (of this Report)

Approved for public release;
distribution unlimited.

17. DISTRIBUTION STATEMENT (of the abstract entered in Block 20, if different from Report)

18. SUPPLEMENTARY NOTES

19. KEY WORDS (Continue on reverse side if necessary and identify by block number)

IR signature suppression; quenching/ radiationless de-excitation; collisional de-excitation

20. ABSTRACT (Continue on reverse side if necessary and identify by block number)

Research directed to assessment of the role of radiationless, collisional de-excitation of excited $CO_2^{\ddagger}$ and $H_2O^{\ddagger}$ in enhancing the effective extinction coefficient of lampblack smokes in air is described. It is found that, unless the $CO_2^{\ddagger}$ or $H_2O^{\ddagger}$ is highly excited, the effect is negligible.

DD FORM 1 JAN 73 1473 EDITION OF 1 NOV 65 IS OBSOLETE

UNCLASSIFIED
SECURITY CLASSIFICATION OF THIS PAGE (When Data Entered)

407 080

Battelle
Columbus Laboratories
505 King Avenue
Columbus, Ohio 43201
Telephone (614) 424-6424